OVERVIEW

Hydrostatic Compression Effects on Fifth-Group Element Superconductors V, Nb, and Ta Subjected to High-Pressure Torsion

Masaki Mito[1,*], Shun Shigeoka[1], Hirotaka Kondo[1], Nozomi Noumi[1], Yuichiro Kitamura[1], Kunihiko Irie[1], Kazuma Nakamura[1], Seishi Takagi[1], Hiroyuki Deguchi[1], Takayuki Tajiri[2], Mamoru Ishizuka[3], Terukazu Nishizaki[4], Kaveh Edalati[5,6] and Zenji Horita[5,6]

[1]*Graduate School of Engineering, Kyushu Institute of Technology, Kitakyushu 804-8550, Japan*
[2]*Faculty of Science, Fukuoka University, Fukuoka 814-0180, Japan*
[3]*Center for Scientific Instrument Renovation and Manufacturing Support, Osaka University, Toyonaka 560-8531, Japan*
[4]*Department of Electrical Engineering, Kyushu Sangyo University, Fukuoka 813-8503, Japan*
[5]*Department of Materials Science and Engineering, Faculty of Engineering, Kyushu University, Fukuoka 819-0395, Japan*
[6]*International Institute for Carbon-Neutral Energy Research (WPI-I2CNER), Kyushu University, Fukuoka 819-0395, Japan*

In fifth-group element superconductors V, Nb, and Ta, the increase in superconducting transition temperature (T_c) was attempted by using both high-pressure torsion (HPT) and additional hydrostatic pressure (HP) compression. The former brings about the grain refinement and strain accumulation in the unit-cell level. The additional compression for severely strained superconductors triggers strengthening intergrain-contact and/or structural deformation in the unit-cell level. The manner of the appearance of the above two effects depends on the kind of elements: First, in V, there is no prominent effect of HPT, comparing to the hydrostatic compression effects on its non-strained material. Next, in Ta, the effect of strengthening intergrain-contact appears at small hydrostatic compression, resulting in temporal increase in T_c. Finally, Nb exhibits prominent increase in T_c by both effects and, in particular, the structural deformation in the unit-cell level promotes the increase in T_c. Thus, the accumulation of residual strain in the level of starting material can be a promising work to manipulate T_c under HP compression.
[doi:10.2320/matertrans.MF201932]

1. Introduction

Bulk superconductivity exhibits macroscopic phase coherence in the Josephson arrays composed of superconducting grains. In late 1950's–early1970's, the superconductivity property at zero magnetic field, ex. superconducting transition temperature T_c, had been found to depend on both the sample purity and residual strain in single element superconductors such as Re,[1] Ta,[2] and V.[3] Generally, the shear strain reduces crystallinity, and it is usually not favorable for macroscopic phase coherence. However, it had been known that it rarely works toward favorable manner in Re,[1] thin film and amorphous Al,[4] and so on. Furthermore when considering the fine-grain superconductors, it has been experimentally confirmed that T_c can increase with strengthening the intergrain coupling.[5,6] This effect is theoretically expected to be enhanced in a system with smaller grain size.[7]

Recently by using severe plastic deformation (SPD),[8,9] the improvement of functionality in superconductors is successfully conducted.[10–12] The SPD process plays the role of accumulating dislocations, resulting in the grain refinement at the submicrometer or nanometer ranges as shown in Fig. 1. It is known to be effective in increasing T_c of superconductors such as Nb[10] and Re.[12] There we have to consider both the intergrain network via grain boundary and intragrain crystallinity as factors to influence T_c. The strain installed in the SPD process is relatively evaluated via semi-experimental manner: In the case of high-pressure torsion (HPT),[13–17] which is one of the SPD techniques along with equal-channel
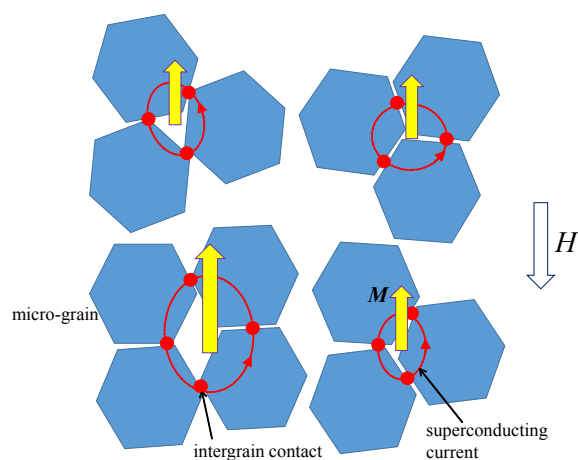

Fig. 1   Intergrain network consisting of superconducting grains. Grains and intergrain-contacts are presented with hexagons and red closed circles, respectively. The diamagnetic moments by the surface current displayed with red dotted curves are presented with yellow arrows. In the magnetic measurements, the summation of yellow M vectors against the magnetic field H is observed.

angular pressing[18] and accumulative roll bonding,[19,20] the revolution number N is a parameter to pursue the grain refinement. In order to elucidate both effects on T_c, we compress three fifth-element superconductors such as V, Nb, and Ta subjected to HPT as illustrated in Fig. 2(a).

In the periodic table containing 118 elements, there are 29 superconductors at ambient pressure, and 11 elements of them exhibit the increase in T_c under hydrostatic pressure (HP).[21,22] Three fifth-element superconductors such as V, Nb, and Ta has nominal T_c of 5.3 K, 9.2 K, and 4.5 K,

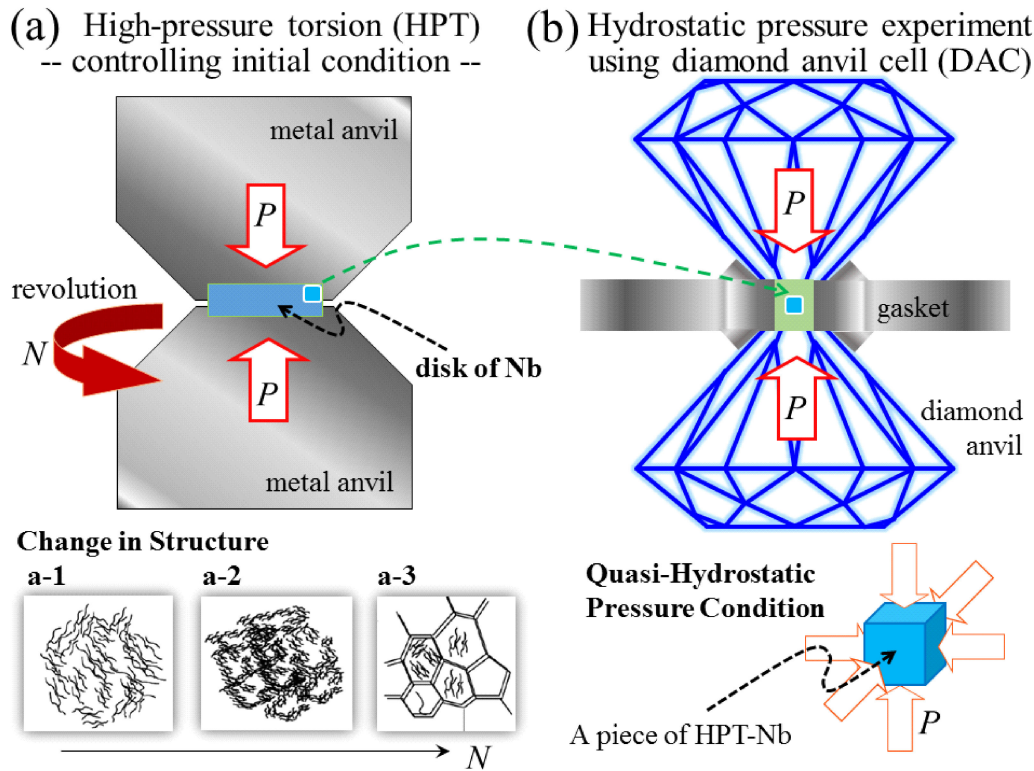*Corresponding author, E-mail: mitoh@mns.kyutech.ac.jp

(a) High-pressure torsion (HPT)
-- controlling initial condition --

metal anvil

P

revolution

N

disk of Nb

P

metal anvil

(b) Hydrostatic pressure experiment
using diamond anvil cell (DAC)

P

gasket

P

diamond anvil

Change in Structure

a-1   a-2   a-3

→ N

Quasi-Hydrostatic Pressure Condition

A piece of HPT-Nb

P

Fig. 2   Strategy of the present study in the case of Nb.[33] (a) In high-pressure torsion (HPT) for controlling the initial condition, pressurization and revolution are conducted by using two metal anvils. As the revolution number (N) increases, dislocations are accumulated (a-1), and the grain size largely changes. The small-angle grain boundaries gradually transform to large-angle grain boundaries with increasing N ((a-2) → (a-3)). Finally due to the balance between generation and annihilation of dislocations, the grain size remains unchanged despite the increase in N. (b) A few pieces of sample cut from the HPT-processed V, Nb, and Ta are placed in diamond anvil cell (DAC) to conduct the hydrostatic pressure experiment. There, the specimen is pressed in a quasi-hydrostatic pressure condition using the DAC.

Table 1   Previous studies on hydrostatic pressure (HP) experiments for V. PTM: pressure-transmitting medium; nP-iA: 1:1 mixture of n-pentane and isoamyl alcohol, and Ap-J: Apiezon-J oil. CY: cylindrical sample, AR: as-received sample, S: single-crystal, SP: small pieces, ARC: arc-melted, and HPT: high-pressure torsion. N denotes the revolution number of the HPT procedure performed at 6 GPa.

year	authors	sample	max. P [GPa]	$T_c(P=0)$ [K]	dT_c/dP [K/GPa]	max. T_c [K]	PTM	ref
1966	Gardner and Smith	CY of AR, ARC	ca. 1	4.92-5.05, 5.20	+0.11	5.31	-	[23]
1968	Köhnlein	-	-	-	+0.176	-	-	[24]
1972	Smith	CY after ARC	2.0	5.272	+0.065	5.40	nP-iA	[3]
1972	Smith	AR	2.3	5.159	+0.061	5.31	nP-iA	[3]
1972	Smith	ARC ball	2.0	4.996	+0.061	5.10	nP-iA	[3]
1972	Smith	disk	2.4	5.475	+0.063	5.62	nP-iA	[3]
1972	Smith	CY	1.9	5.469	+0.059	5.59	nP-iA	[3]
1972	Smith	disk from S	2.3	5.036	+0.063	5.19	nP-iA	[3]
1973	Brandt and Zarubina	-	18	-	c.a +0.1	7.2	-	[25]
1995	Akahama $et\ al.$	SP, high purity	50	5.3	+0.096	9.5	pyrophyllite	[26]
2000	Ishizuka $et\ al.$	SP	120	5.3	+0.1	17.2	none	[27]
2019	present work	HPT ($N=0$)	5.0	5.42	+0.12	5.9 (5 GPa)	Ap-J	-
2019	present work	HPT ($N=10$)	32.0	5.41	+0.12	10.4 (32 GPa)	Ap-J	-

respectively. Previous studies of HP compression for V, Nb, and Ta are summarized in Tables 1, 2, and 3, respectively. All of three are considered to belong to a group that exhibits the increase in T_c under the HP circumstances.[22] Indeed, smooth

linear-increase in T_c is observed only in V. All previous studies for V have reported the positive dT_c/dP coefficient.[3,23–27] According to the study of Struzhkin $et\ al.$, non-strained Nb shows the increase in T_c after its slight decrease,

Table 2   Previous studies on HP experiments for Nb. PTM: pressure-transmitting medium; nP-iA: 1:1 mixture of n-pentane and isoamyl alcohol, Ap-J: Apiezon-J oil, MEW: methanol–ethanol–water mixture in volume ratio of 16:3:1, and O_2: condensed oxygen molecule. CY: cylindrical sample, AR: as-received sample, S: single-crystal, PO: polycrystal, SP: small pieces, PU: purified near the melting point, ARC: arc-melted, and HPT: high-pressure torsion. N denotes the revolution number of the HPT procedure performed at 6 GPa.

year	authors	sample	max. P [GPa]	$T_c(P=0)$ [K]	initial dT_c/dP [K/GPa]	ΔT_c [K]	max. T_c [K]	PTM	ref
1966	Gardner and Smith	CY of AR	ca. 1	9.43, 9.52	ca. 0	-	-	-	[23]
1966	Gey and Heyden	-	2.5	9.4, 9.5	ca. -0.03	-	-	-	[29]
1968	Köhnlein	-	4.1	9.40	+0.012	0.31	9.71 (4 GPa)	-	[24]
1969	Gey	PU	7.3	-	+0.11	0.23	-	-	[30]
1970	Brandt and Papp	CY	1.6	9.1	-	<0.1	-	kerosene-oil	[31]
1970	Smith	S, PO	2.4	9.15-9.21	$-0.016 - -0.025$	-0.05	-	nP-iA	[32]
1997	Struzhkin *et al.*	SP	70	ca. 9.2	-0.025	0.7	9.9 (10 GPa)	NaCl	[28]
1997	Struzhkin *et al.*	SP	132	ca. 9.2	-	0.7	9.8 (15 GPa)	none	[28]
2019	Mito *et al.*	AR	15.0	9.35	+0.09	0.38	9.78 (15.0 GPa)	Ap-J	[33]
2019	Mito *et al.*	ARC	6	9.05	+0.14	0.26	9.31 (ca. 2 GPa)	Ap-J, MEW	[33]
2019	Mito *et al.*	HPT ($N=1$)	6.0	9.35	+0.61	0.49	9.84 (ca. 1 GPa)	Ap-J	[33]
2019	Mito *et al.*	HPT ($N=2$)	14.6	ca. 9.35	+0.33	0.38	9.79 (14.6 GPa)	Ap-J	[33]
2019	Mito *et al.*	HPT ($N=5$)	10.1	ca. 9.35	+0.18	0.36	9.72 (ca. 2 GPa)	Ap-J	[33]
2019	Mito *et al.*	HPT ($N=10$)	14.6	ca. 9.35	+0.29	0.57	9.92 (2.2 GPa)	Ap-J	[33]
2019	Mito *et al.*	HPT ($N=10$)	6.2	ca. 9.35	+0.19	0.43	$\geq$9.78 (6.2 GPa)	MEW	[33]
2019	Mito *et al.*	HPT ($N=10$)	4.3	ca. 9.35	+0.03	0.08	9.43 (3.5 GPa)	O_2	[33]
2019	Mito *et al.*	HPT ($N=10$)(cryo)	5.0	9.54	+0.18	0.38	9.92 (2.8 GPa)	Ap-J	[33]
2019	Mito *et al.*	HPT ($N=20$)	5.6	ca. 9.35	+0.24	0.50	9.85 (2.4 GPa)	Ap-J	[33]

Table 3   Previous studies on HP experiments for Ta. PTM: pressure-transmitting medium; Ap-J: Apiezon-J oil, SP: small pieces, and HPT: high-pressure torsion. N denotes the revolution number of the HPT procedure performed at 6 GPa.

year	authors	sample	max. P [GPa]	$T_c(P=0)$ [K]	initial dT_c/dP [K/GPa]	max. T_c [K]	PTM	ref
1956	Hatton	moderately annealed	0.5	4.385	$-0.025 \sim -0.053$	-	-	[34]
1958	Jennings and Swenson	2300 C° annealed	ca. 1	4.305	-0.026	-	solid H_2	[2]
1968	Kohnlein	-	3.6	4.43	-0.026	-	-	[24]
1997	Struzhkin *et al.*	SP	43	4.43	-0.022	4.5 (43 GPa)	none	[28]
2019	present work	HPT ($N=0$)	6.0	4.40	+0.045	4.44	Ap-J	-
2019	present work	HPT ($N=0.5$)	9.5	4.367	+0.004	4.372	Ap-J	-
2019	present work	HPT ($N=2$)	4.7	4.42	+0.015	4.45	Ap-J	-
2019	present work	HPT ($N=5$)	6.9	4.37	-0.058	4.41	Ap-J	-
2019	present work	HPT ($N=10$)	8.8	4.36	+0.056	4.42	Ap-J	-

and has the optimal T_c of 9.9 K at around $P = 10$ GPa.[28] Indeed, the initial dT_c/dP for Nb depends on experimental conditions such as the sample condition and kind of pressure transmitting medium (PTM).[23,24,28–33] Contrary to the above two, Ta exhibits the decrease in T_c over wide pressure range,[2,24,28,34,35] and there is only one plot suggesting the increase in T_c at 43 GPa.[28] Thus, there are much variety in the pressure dependence of T_c among V, Nb, and Ta. We are exploring the observation of new pressure response using the SPD materials. In the present study, we conduct the HP compression to strained materials subjected to the HPT process (see Fig. 2), considered as the so-called Josephson arrays of small grains, and control both Josephson coupling between superconducting grains and lattice strain at the unit-cell level. Figure 3 shows a digest of the present review. There are two parameters such as N related with the initially installed strain [Fig. 2(a)] and pressure (P) related with additional strain [Fig. 2(b)]. Both HPT apparatus and HP one commonly using anvils have the same route of Bridgman's excellent achievement.[13]
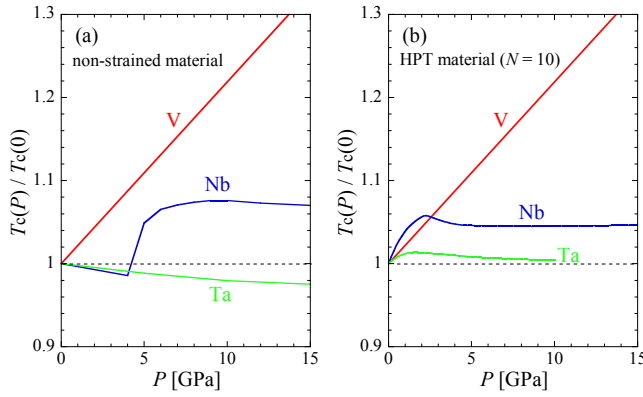
Fig. 3 Digest of the present studies for fifth-element transition-metal superconductors, V, Nb, and Ta. The pressure dependences of T_c normalized with the value at ambient pressure, $T_c(0)$, for $P \leq 15$ GPa are presented in two cases of (a) non-strained material and (b) material subjected to the HPT procedure with $N = 10$ at 6 GPa.

2. Experimentals

2.1 High-pressure torsion (HPT)

As illustrated in Fig. 2(a), the disks of V, Nb, and Ta were subjected to HPT processing at room temperature under a selected pressure of $P = 6$ GPa and revolutions of N up to 20 with a rotation speed of 1 rpm. Specimens with dimensions of approximately $0.8 \times 0.8 \times 0.5$ mm^3 were cut from an HPT-processed disk using a wirecutting electric discharge machine at the position of 2.5 mm from the disk center. For instance, in Nb, we remark that for $N < 2$, dislocations are stored as illustrated in Fig. 2(a-1), and the grain size largely changes.[36] The small-angle grain boundaries formed in these cases gradually transform to large-angle grain boundaries with increasing N (corresponding to the change form Fig. 2(a-2) to Fig. 2(a-3)). On the other hand, for $N \geq 2$, the fraction of large-angle grain boundaries increases due to annihilation of dislocations at grain boundaries (illustrated in Fig. 2(a-3)), leading to that the grain size remains unchanged because of the balance between dislocation generation by straining and the dislocation annihilation at grain boundaries. The grain size at steady state for V, Nb, and Ta is 330 nm, 240 nm, and 180 nm, respectively.[37]

In Nb, we note here that the average grain sizes for AR, $N = 2$, $N = 5$, and $N = 10$(cryo) samples have been reported to be 140 μm, 250 nm, 240 nm, and ca. 40 nm, respectively.[36,38] Thus, the shear insertion leads to a significant reduction in the grain size. The superconducting coherence length $\xi(0)$ for the single-crystal has been reported as around 20 nm,[39] and the aforementioned grain sizes for $N = 2$, $N = 5$, and $N = 10$(cryo) are at a level comparable with $\xi(0)$.[10] The penetration depth for the single-crystal is approximately 40 nm,[39] and large superconducting signal observed in the present study reflects the intergrain coupling via grain boundaries. At ambient pressure, T_c for AR is approximately 9.25 K, and T_c exhibits a maximum of approximately 9.37 K at $N = 2$. In addition, T_c remains unchanged at 9.35 K for $N > 10$.[10]

For the following hydrostatic experiment, small pieces with side lengths less than 0.1 mm were prepared from the specimens with dimensions of approximately $0.8 \times 0.8 \times$

0.5 mm^3 as illustrated in Fig. 2. As for Ta, it has been known that Ta subjected to the HPT processing has two superconducting transitions.[40] The Meissner signal with lower T_c exhibits majority of superconducting volume fraction. In the present experiment using little sample volume, it was difficult to pursue the change in the Meissner signal with higher T_c under HP compression. Thus, for HPT-Ta, we have paid much attention to the change in the Meissner signal with lower T_c that exhibits the same pressure dependence as that for the midpoint of the Meissner signal. In the electrical resistance measurements for superconductors under high pressure, it is difficult to measure zero resistance. In particular, this problem becomes more serious in strained superconductors under non-HP compression. Therefore, we adopt the Meissner measurements to evaluate T_c of V, Nb, and Ta in the present extreme condition.

2.2 SQUID magnetometer with miniature-DAC (mDAC)

The AC magnetization of the materials at pressures of GPa level was measured using a superconducting quantum interference device (SQUID) magnetometer equipped with an AC option.[41–47] The frequency and amplitude of the AC field were 10 Hz and 3.9 Oe, respectively. At small amplitude of AC field, the magnitude of in-phase one (m') is almost consistent with the Meissner signal observed at static magnetic field.[48] Sufficiently below T_c, there is no out-of-phase component reflecting energy loss, and m' is related with the volume fraction of magnetic shielding. The onset temperature of the superconducting signal was evaluated as the confident T_c after the quantitative deviation of the onset temperature was confirmed to be consistent with that of the midpoint temperature.

Contraction corresponding to a stress of up to 15 GPa was achieved using a miniature CuBe diamond anvil cell (DAC) that consisted of two diamond anvils with flat tips having a diameter of 0.5 mm and a 0.25-mm-thick Re gasket.[49,50] In the HP-type experiments, liquid-like PTM, Apiezon-J oil (Ap-J), was confined together with small pieces of the HPT materials in the sample chamber: At room temperature, Apiezon-J oil solidifies at a few one-tenth GPa. The pressure value at room temperature (P_{rt}) was evaluated by measuring the fluorescence of ruby[51] located in the sample cavity with the HPT materials. According to Ref. 49, when temperature is cooled from room temperature to liquid helium temperature, there appears the pressure increase equal to approximately 10% of P_{rt}. In this paper, P_{rt} is adopted as the pressure value (P) in each measurement, since the comparison between magnetic and structural data at low pressures of $P < 7$ GPa is meaningful.

2.3 SQUID-based vibrating coil magnetometer (SQUID-VCM)

The DAC is mounted in the ^{4}He-refrigerator with a 1 K pot, and the entire DAC is heated. The use of diamond anvils with different culet size (i.e. 500 and 550 μm) allows the CuBe–NiCrAl composite gasket to be deformed away from the NbTi detection coil. The NiCrAl disk with the diameter of 410 μm was inserted into the hole drilled in the center of CuBe gasket.[52] After pressing the composite gasket down to

70 µm, a hole with the diameter of 200 µm was drilled in the center. In the sample cavity, the small pieces of HPT-V ($N = 10$) were held together with Apiezon-J oil and ruby as a room-temperature manometer. The magnitude of the pressure (P) was estimated at room temperature by measuring the fluorescence of ruby.[51]

Using an actuating unit consisting of three actuators, the detection coil is ideally vibrated at the place where the slope of magnetic flux against the distance from the sample is maximum.[53] To obtain sufficient amplitude of the vibration of the detection coil at liquid helium temperature, the driving frequency of the vibrating actuators, consisting of bimorph type piezoelectric actuators, was chosen to be 168 Hz near the resonating frequency of the vibrating actuators.[54] The DAC and the actuating unit are located in the cryostat as shown elsewhere.[54] H_{dc} was applied at 30 Oe at maximum. The use of a lock-in amplifier at the vibration frequency yields the amplitude of V_{VCM}.

2.4 X-ray diffraction under hydrostatic compression

In order to determine the structural shrinkage under pressure, we performed X-ray diffraction (XRD) analyses for Nb and Ta under high pressure of up to $P = 6.8$ GPa at room temperature using a synchrotron radiation XRD system with a cylindrical imaging plate at the Photon Factory at the Institute of Materials Structure Science, High Energy Accelerator Research Organization.[55] The energy of the incident X-rays was 16 keV. Pressure was applied using a DAC that consisted of two diamond anvils with flat tips having a diameter of 0.8 mm and a 0.3-mm-thick CuBe gasket. The small pieces of HPT-Nb or HPT-Ta were placed in a randomly oriented manner in a sample cavity with a diameter of 0.4 mm along with a ruby of manometer and transparent PTM such as fluorinated oil (FC77, Sumitomo 3M Ltd.). Transparent FC77 undergoes solidification below 1 GPa at room temperature[56] similarly to brown Ap-J. All the atomic positions in the body-centered cubic (bcc) structure are special positions, and therefore, the structural parameters can be evaluated just with the use of the diffraction peak angle. The lattice parameters were estimated using all of observed diffraction peaks: For Nb, we used five diffraction peaks of the plane indices (110), (200), (211), (220), and (310). For Ta, the diffraction peak of the plane index (310) was not used.

3. Experimental Results

3.1 HPT-V

Figure 4 shows the temperature dependence of in-phase ac magnetization m' for HPT-V ($N = 0$) (a) and HPT-V ($N = 10$) (b) by using a SQUID magnetometer with miniature-DAC (mDAC). Figure 5 shows V_{VCM} that corresponds to the temperature dependence of dc magnetic susceptibility for HPT-V ($N = 10$) by using the SQUID-VCM magnetometer. Figure 6 shows the pressure dependence of T_c for HPT-V ($N = 0$) and HPT-V ($N = 10$). Comparing T_c's at $P = 5.0$ GPa, HPT-V ($N = 10$) has slightly higher value than HPT-V ($N = 0$). However, when we see their data in wider pressure range, there is no prominent difference in the change in T_c between HPT-V ($N = 0$) and HPT-V ($N = 10$), which are consistent with the previous data by Ishizuka *et al.*[27]
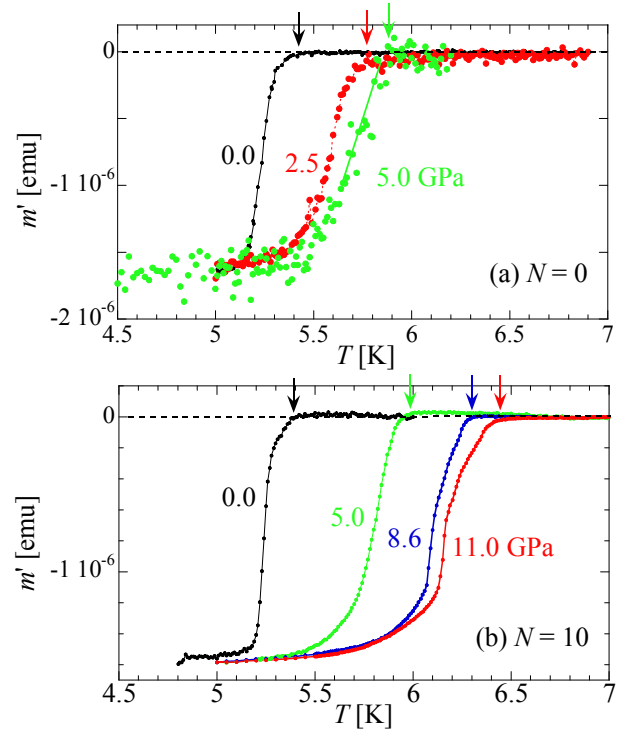
Fig. 4 Temperature dependence of in-phase ac magnetization m' for HPT-V ($N = 0$) (a) and HPT-V ($N = 10$) (b).
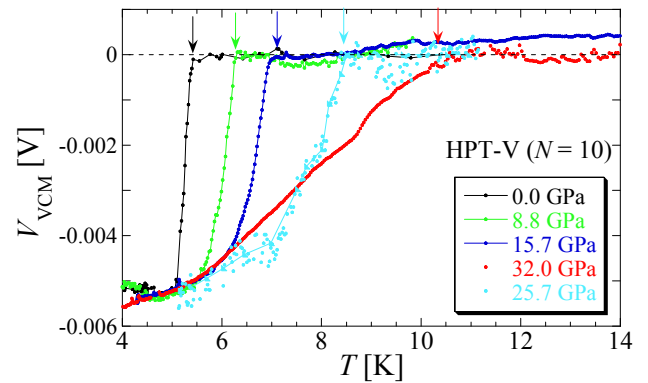
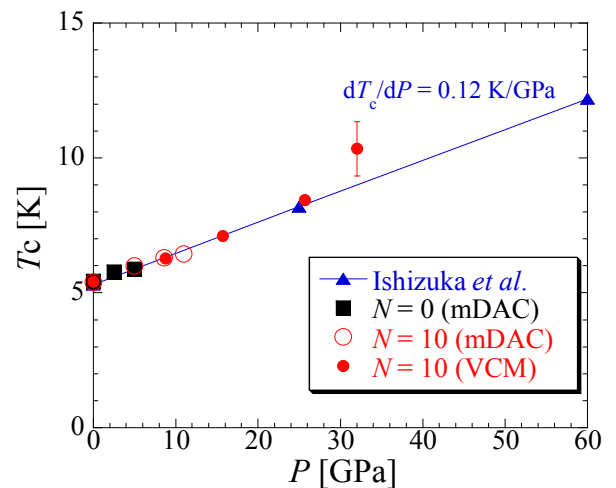Fig. 5 Temperature dependence of dc magnetic susceptibility for HPT-V ($N = 10$).

Fig. 6 Pressure dependence of superconducting transition temperature T_c for HPT-V ($N = 0$) and HPT-V ($N = 10$). For reference, the previous data for non-strained V are also presented.[27]
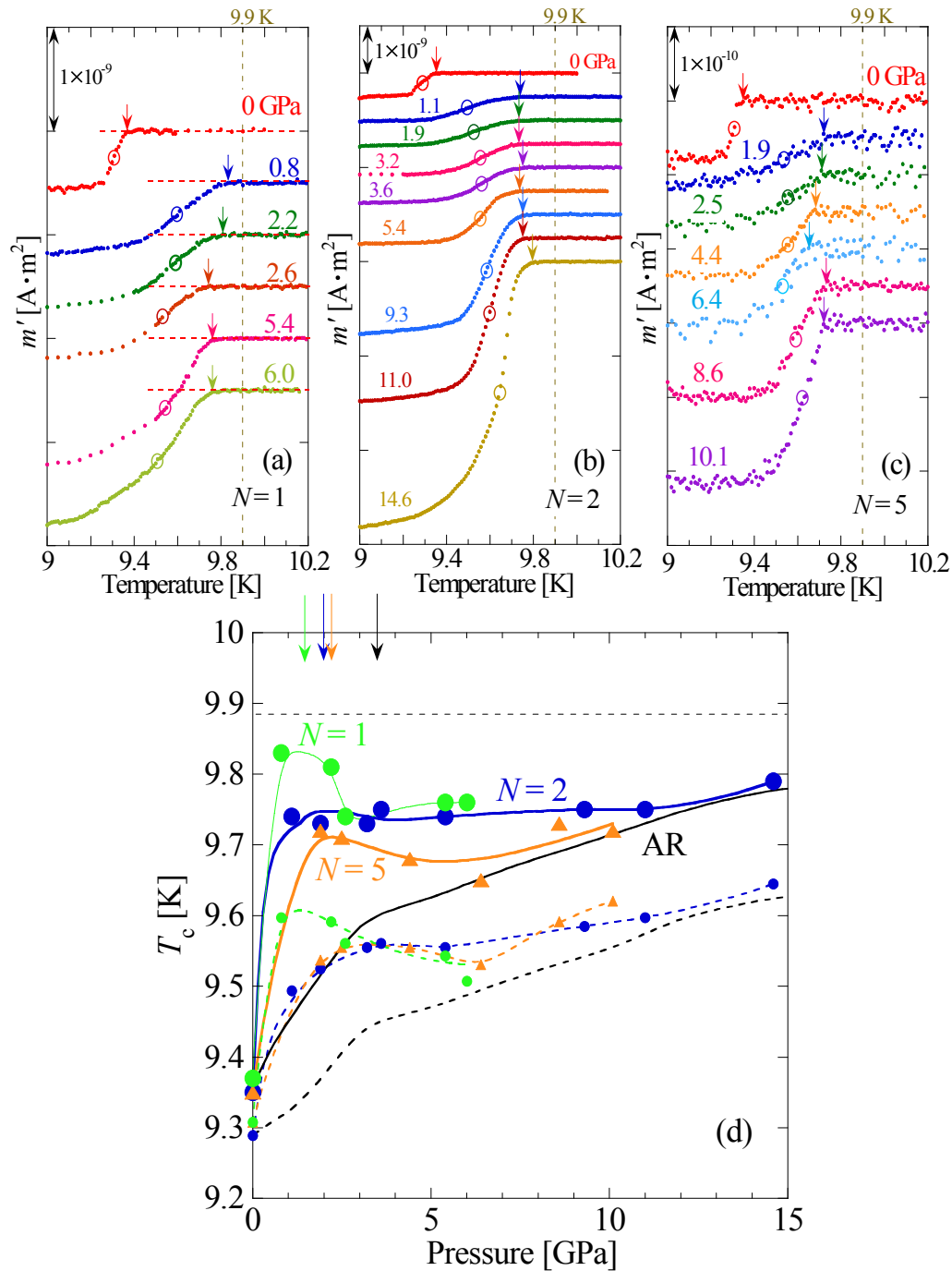
Fig. 7 Temperature dependence of in-phase ac magnetization m' for HPT-Nb samples with $N = 1$ (a), 2 (b) and 5 (c) at various pressures.[33] The diameter of the sample chamber for $N = 1$ and 2 was 0.2 mm, and that for $N = 5$ was 0.1 mm. The onset of the superconducting signal is presented with an arrow, and the midpoint is marked with an open circle. (d) Pressure dependence of superconducting transition temperature T_c for HPT-Nb for $N = 1$, 2, and 5. Arrows represent the threshold pressure (P_c). For three samples, Ap-J was used as the PTM. For reference, the guide curves corresponding to $T_c(P)$ of the AR sample with Ap-J as the PTM (see Ref. 33) are also presented with the black solid (onset) and broken (midpoint) curves.

3.2   HPT-Nb

Figures 7(a)–(c) shows the temperature dependence of in-phase ac magnetization m' for the HPT-Nb ($N = 1$, 2, and 10) materials by using a SQUID magnetometer with mDAC. The onset of the Meissner signal shows the change similar to that of the midpoint, and the onset temperature is determined to be T_c. The pressure dependence of T_c for HPT-Nb ($N = 1$, 2, and 10) is shown in Fig. 7(d), comparing to that of as-received (AR) Nb material. Three HPT materials exhibit the larger enhancement of T_c than the AR material. In particular, HPT-Nb ($N = 1$) shows the increase in T_c over 9.8 K at around $P = 1$ GPa. As N increases like $N = 1 \rightarrow 5$, the maximum T_c shifts toward higher pressure side, decreasing the maximum value.

Figures 8(a)–(c) shows the temperature dependence of in-phase ac magnetization m' for the HPT-Nb ($N = 10$) material by using a SQUID magnetometer with mDAC. The pressure dependence of the onset temperature T_c for HPT-Nb ($N = 10$)
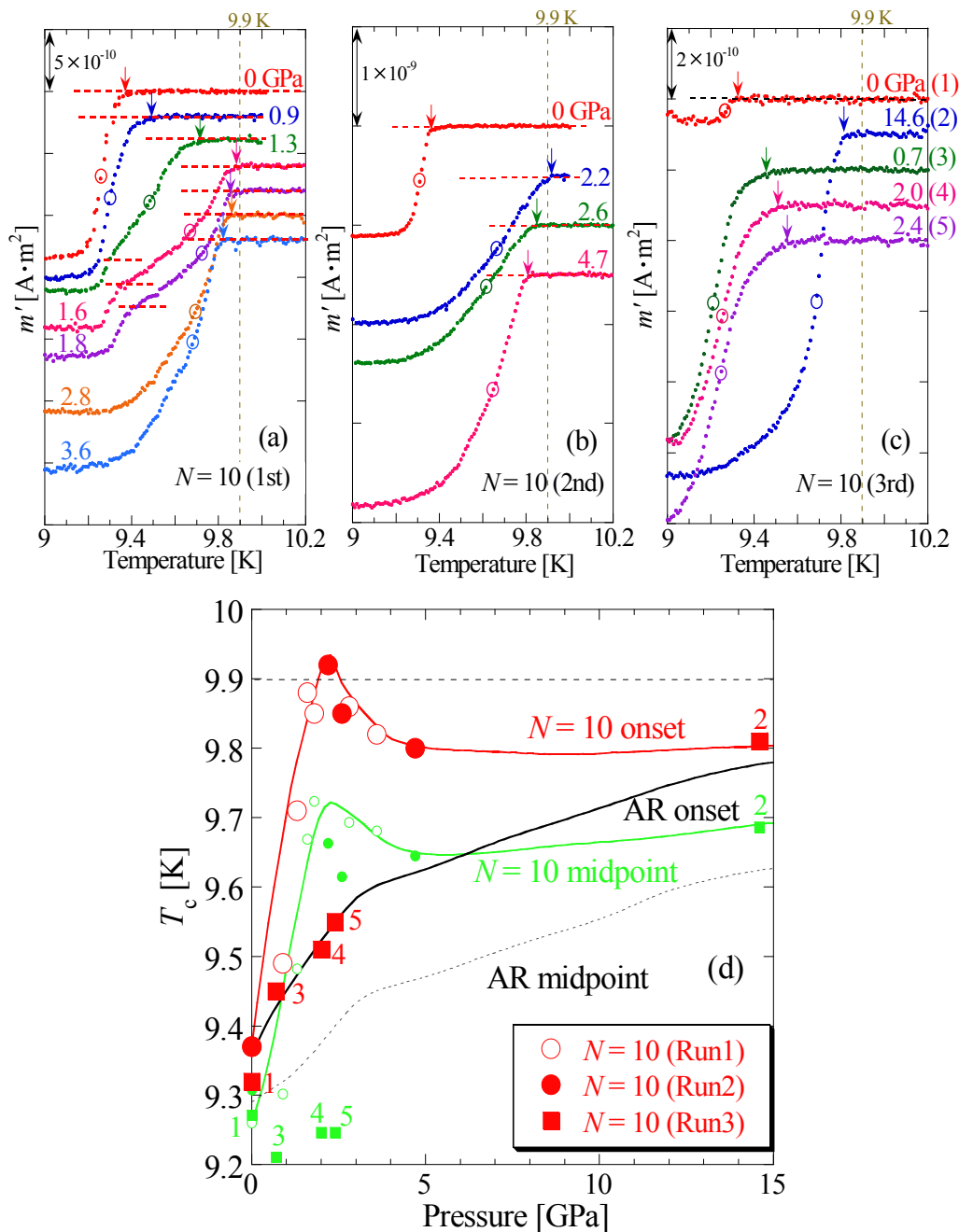
Fig. 8 Temperature dependence of in-phase ac magnetization m' for HPT-Nb samples with $N = 10$ using Ap-J as PTM [first run (a), second one (b), and third one (c)] at various pressures.[33] The diameter of the sample chamber for the first and second runs was 0.2 mm, and that for the third run was 0.1 mm. The onset of the superconducting signal is presented with an arrow, and the midpoint is marked with an open circle. For $P = 1.3$, 1.6, and 1.8 GPa in (a), the midpoint was evaluated for the major superconducting signal. The number beside the pressure value in the figure indicates the measurement trial number. (d) Pressure dependence of superconducting transition temperature T_c for HPT-Nb with $N = 10$. Here, Ap-J was used as the PTM. The number beside each symbol indicates the measurement trial number. For reference, the guide curves corresponding to $T_c(P)$ of the sample AR using Ap-J as PTM (see Ref. 33) are also presented with the black solid (onset) and broken (midpoint) curves.

is shown in Fig. 8(d). T_c of HPT-Nb ($N = 10$) exhibits the maximum T_c over 9.8 K at around $P = 2$ GPa. The behavior of T_c for HPT-Nb ($N = 10$) is not on an expanded line of changes for $N = 1 \rightarrow 5$. T_c for all HPT-Nb ($N = 1, 2, 5, 10$) materials shows consistency with that for AR at around $P = 15$ GPa. The feature due to the HPT processing appears in the pressure region below 15 GPa.

Figures 9 shows the pressure dependence of interplanar distance of (110), (200), (211), (220), and (310) for the HPT-Nb materials for $N = 1$ (c) and 10 (d). For reference, the data

for both arc-melting (ARC) and AR materials are also shown in Figs. 9(a) and 9(b), respectively. At first, the AR material exhibits anisotropic transformation of the unit cell structure at around $P = 2$ GPa, suggesting that strain accumulated in the cubic lattice with high symmetry is released at a threshold pressure (P_c). This phenomenon does not occur in the ARC material without residual strain, suggesting the importance of residual strain. When the HPT procedure with $N = 1$ is subjected to the AR material, the grain refinement enhances the capacity of accumulating the additional strain, resulting in
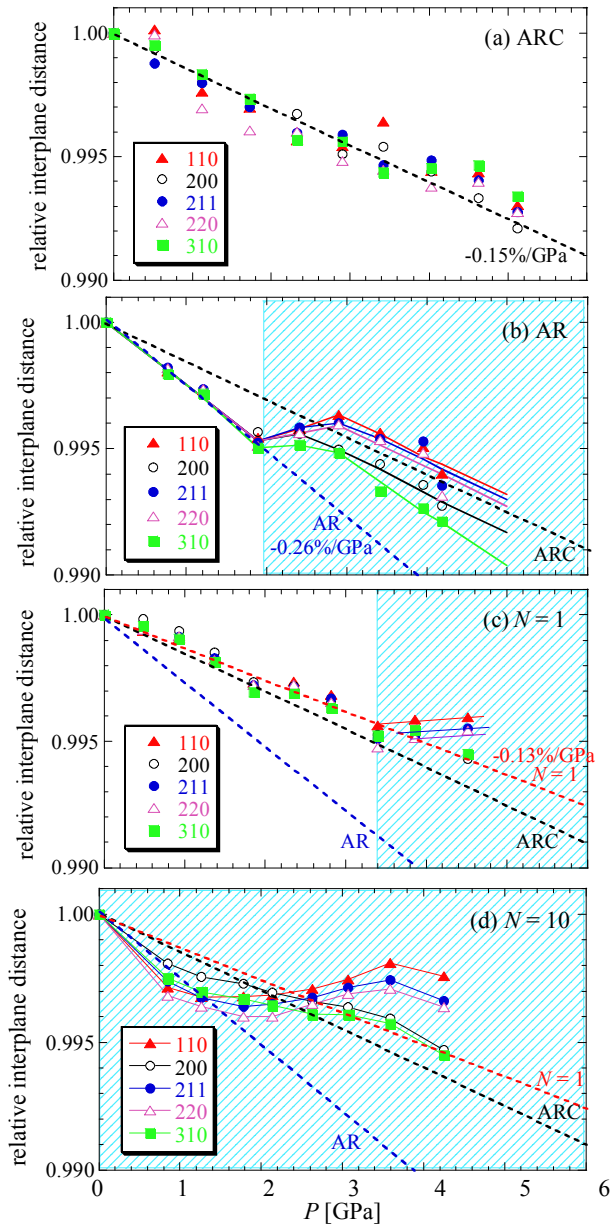
Fig. 9 Pressure dependence of normalized interplanar distance of (110), (200), (211), (220), and (310) planes for ARC (a), AR (b), HPT-Nb ($N = 1$) (c), and HPT-Nb ($N = 10$) (d).[33] The broken guide lines in all figures represent the interplanar distance change for ARC (black), AR (blue), and $N = 1$ (red). These initial slope values in the pressure regime where isotropic structure change occurs are also indicated. The pressure regime corresponding to anisotropic structure change is indicated in light-blue hatching. FC77 was used as PTM in all cases.

Fig. 10 Pressure dependence of anisotropic lattice deformation using normalized lattice constants a_1/a_{cubic}, a_2/a_{cubic}, and a_3/a_{cubic} for ARC (a), AR (b), HPT-Nb ($N = 1$) (c), and HPT-Nb ($N = 10$) (d).[33] a_{cubic} is a lattice constant considering the bcc lattice. The threshold pressure for anisotropic structure change, determined in Fig. 9, is indicated by an arrow. FC77 was used as the PTM in all cases.

the increase in P_c to approximately 3.4 GPa. However, HPT with the level of $N = 10$ does not permit to accumulate any additional strain, so that anisotropic unit-cell deformation occurs even at quite small pressure.

Figure 10 shows the pressure dependence of anisotropic lattice deformation using normalized lattice constants a_1/a_{cubic}, a_2/a_{cubic}, and a_3/a_{cubic} for ARC (a), AR (b), HPT-Nb ($N = 1$) (c), and HPT-Nb ($N = 10$) (d) samples. Herein, a_{cubic} is a lattice constant considering the bcc lattice. Comparing with ARC, AR and HPT ($N = 1$) exhibits the one-direction shrinkage and two-direction expansion. On the other hand, the HPT ($N = 10$) material exhibits two-direction
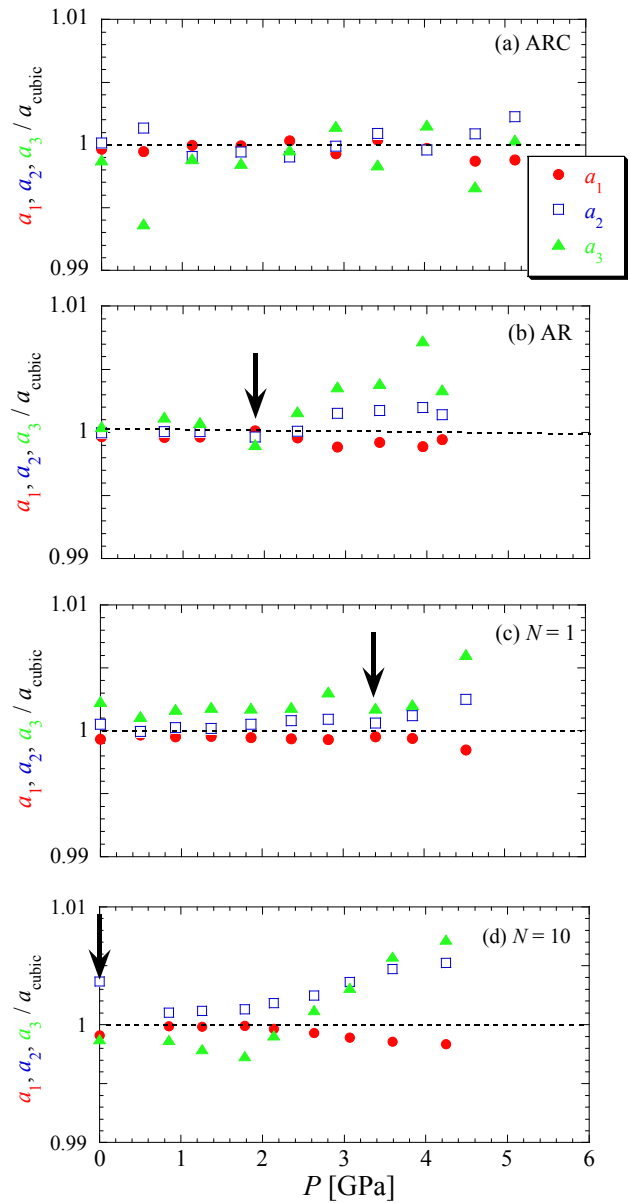
shrinkage for $P < 2$ GPa and two-direction expansion for $P > 2$ GPa. At around 2 GPa, the deformation manner changes, suggesting complex manner of strain release. In particular, the HPT ($N = 10$) material with heavy residual strain has a deformed bcc structure, which is close to the body-centered tetragonal (bct) structure for $P > 3$ GPa.

3.3 HPT-Ta

Figures 11, 12, and 13 shows the temperature dependence of in-phase ac magnetization m' for the HPT-Ta ($N = 0$, 2, and 10) materials by using a SQUID magnetometer with mDAC. The onset of the Meissner signal is determined to be T_c. The pressure dependence of T_c for HPT-Ta ($N = 0$, 2, and 10) is shown in Fig. 14, comparing to the previous data for
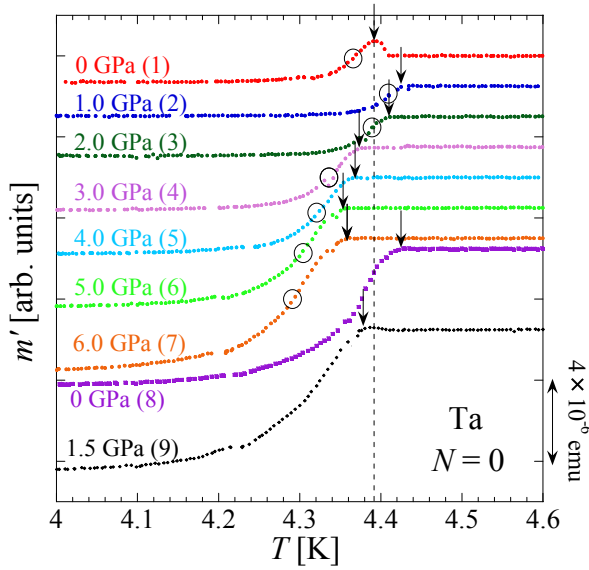
Fig. 11 Temperature dependence of in-phase ac magnetization m' for HPT-Ta with $N = 0$ using Ap-J as PTM at various pressures. The diameter of the sample chamber was 0.2 mm. The onset of the superconducting signal is presented with an arrow, and the midpoint is marked with an open circle. The number beside the pressure value in the figure indicates the measurement trial number.
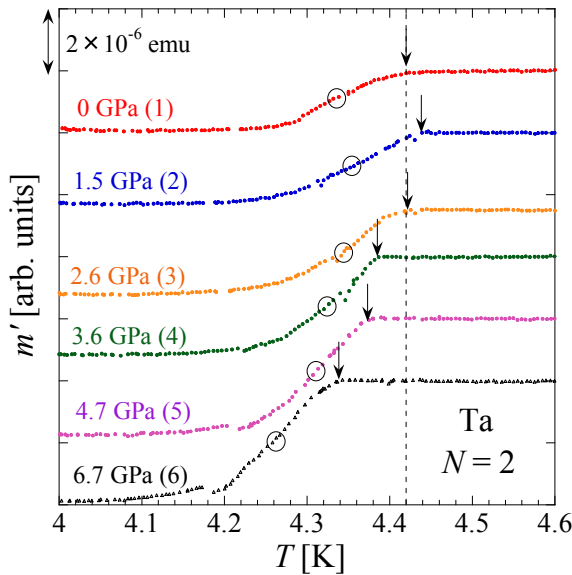

Fig. 13 Temperature dependence of in-phase ac magnetization m' for HPT-Ta with $N = 10$ using Ap-J as PTM at various pressures. The diameter of the sample chamber was 0.2 mm. The onset of the superconducting signal is presented with an arrow, and the midpoint is marked with an open circle. The number beside the pressure value in the figure indicates the measurement trial number.

Fig. 12 Temperature dependence of in-phase ac magnetization m' for HPT-Ta with $N = 2$ using Ap-J as PTM at various pressures. The diameter of the sample chamber was 0.2 mm. The onset of the superconducting signal is presented with an arrow, and the midpoint is marked with an open circle. The number beside the pressure value in the figure indicates the measurement trial number.

Fig. 14 Pressure dependence of superconducting transition temperature T_c for HPT-Ta ($N = 0$, 0.5, 2, 5, and 10) materials. For reference, the previous data for non-strained Ta are also presented with black broken curve.[28] For $N = 5$, the closed circles stand for the data in the pressure-increasing process up to 6.9 GPa, and the open circles do for those in the pressure-increasing process after releasing the pressure of 6.9 GPa.

non-strained Ta.[28] All of three HPT materials exhibit the maximum T_c at around $P = 1$–2 GPa. For $P < 2$ GPa, HPT ($N = 2$) shows the highest T_c among three, whereas for $P > 2$ GPa, HPT ($N = 10$) does the highest T_c. HPT ($N = 0.5$) with initial accumulation of dislocation exhibits little increase in T_c. HPT ($N = 5$) with competition of small-angle grain boundaries and large-angle grain boundaries exhibits strange down-up-down-up-down change in T_c. These behaviors suggests that intergrain network becomes a key factor to determine T_c.
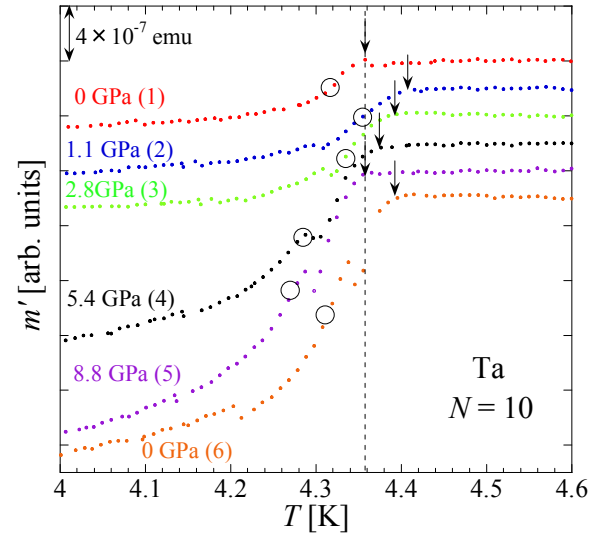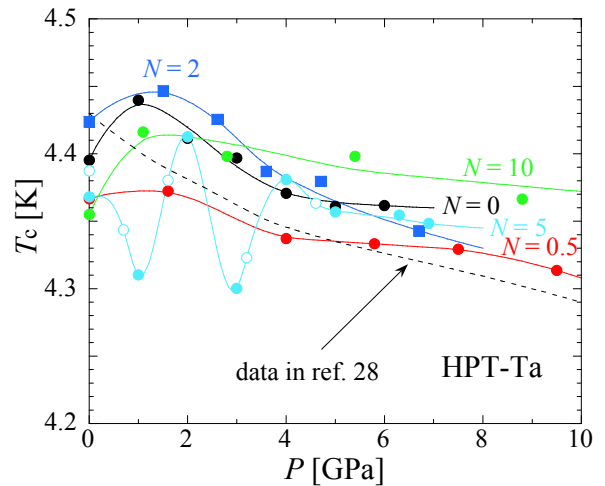
Figures 15 shows the pressure dependence of interplanar distance of (110), (200), (211), and (220) for the HPT-Ta samples for $N = 0$ (a), 2 (b), and 10 (c). In all of three, all of interplanar distances exhibit the shrinkage, and there are no anisotropic deformation of the bcc unit cell. For $N = 0$, at around $P = 1$–2 GPa, the shrinkage magnitude is suppressed similarly to that observed in AR-Nb. The above pressure region is consistent with that possessing the maximum of T_c. On the other hand, both $N = 2$ and 10 shows that the uniform contraction continues monotonously. Both HPT ($N = 2$) and HPT ($N = 10$) do not show anomalous change in a at around $P = 1$–2 GPa, suggesting that the increase in T_c cannot be explained only with the change in lattice constant. Figure 16 shows the pressure dependence of normalized lattice constant
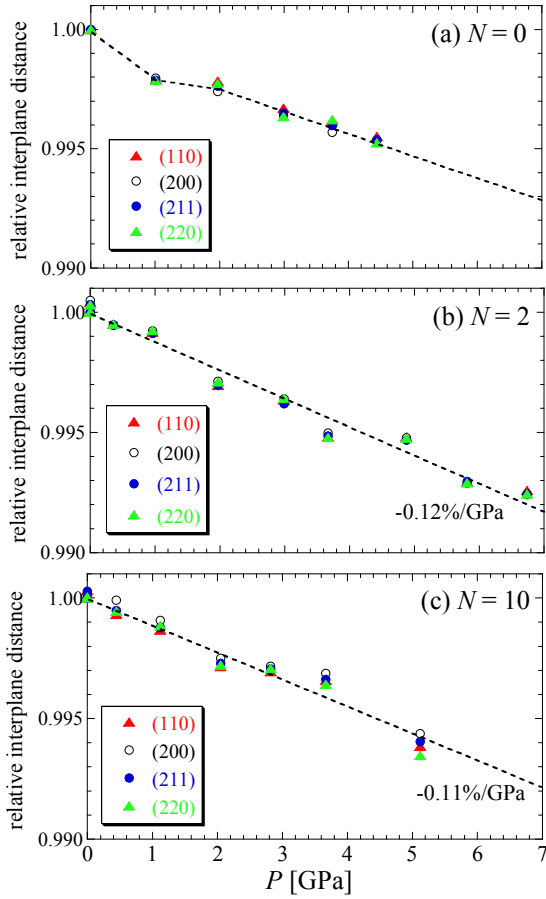
Fig. 15 Pressure dependence of normalized interplanar distance of (110), (200), (211), and (220) planes for HPT-Ta with $N = 0$ (a), 2 (b), and 10 (c).
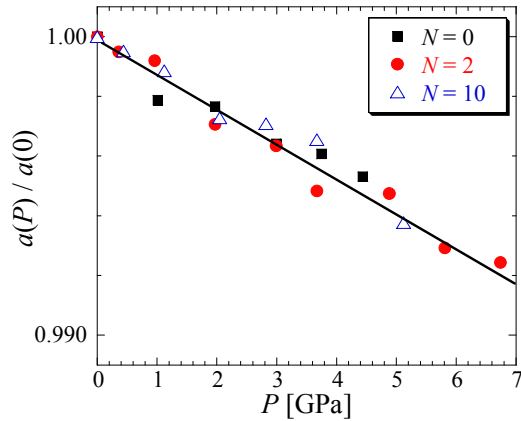

Fig. 16 Pressure dependence of lattice constant of the bcc lattice for HPT-Ta with $N = 0$, 2, and 10. The lattice constant a is normalized with the value at ambient pressure. The solid line has the slope of -1.2×10^{-3} K/GPa.

a. There is no prominent N dependence, and a continues to decrease monotonously in the considered pressure region.

4. Discussion

4.1 Josephson contact

In the HPT procedure, the shear stress inserts dislocations and reduces crystallinity, resulting in the grain refinement at the submicrometer or nanometer ranges as shown in Fig. 1.
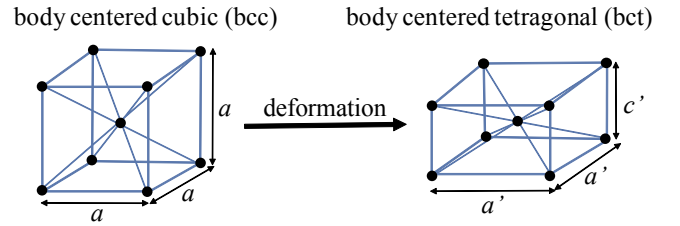

Fig. 17 Schematic of lattice deformation, where a bcc lattice (left panel) is deformed to a bct lattice (right).[33]

The additional HP compression reduces the intergrain space, and strengthens the intergrain coupling. It has already been confirmed in the experimental side that T_c can increase with strengthening the intergrain coupling.[5,6] This effect is theoretically suggested to be enhanced in a system with smaller grain size.[7] We assume that the aforementioned effect appears prominently for HPT-Nb ($N = 1$) and all HPT-Ta ($N = 0$, 2, and 10) materials.

4.2 Anisotropic unit-cell compression ∼Change in Density of State by Deforming Lattice∼

We have to consider another mechanism for increasing T_c for the HPT-Nb ($N = 10$) materials. According to another work,[33] sharp increase in T_c for HPT-Nb ($N = 10$) using the Apiezon-J grease does not appear in the case of good HP condition using MEW and O_2. The maximum T_c for HPT-Nb ($N = 10$) using the Apiezon-J oil should be related with the anisotropic contraction of the unit cell. Thus, it is of interest to understand whether or not the anisotropic structure change from bcc to the orthorhombic system close to the tetragonal lattice actually leads to the increase in T_c.

We performed density-functional calculations for Nb using the extended version of the Tokyo Ab-initio Program Package[57] with plane-wave basis sets, where norm-conserving pseudopotentials[58,59] and the generalized gradient approximation of the exchange-correlation potential[60] were employed. The cutoff energies in the wavefunction and charge densities were 64 and 256 Ry, respectively, and $40 \times 40 \times 40$ k-point sampling was employed. The electronic density of states (DOS) was calculated by means of the generalized tetrahedron method.[61,62]

Based on experimental trends in the lattice change, we first focus on the specific deformation of the bcc structure to the bct structure, which is schematically shown in Fig. 17. The deformation is expressed as $(a, a, a) \to (a', a', c')$ with $a' = (1 + \delta)a$ and $c' = (1 - \delta)a$. In the present calculation, we assume $a = 3.29$ Å and $\delta = 0.015$. The Bravais lattice is expressed for a bcc system as,

$$\mathbf{a}_1 = \frac{a}{2}(-1, 1, 1),$$

$$\mathbf{a}_2 = \frac{a}{2}(1, -1, 1),$$

$$\mathbf{a}_3 = \frac{a}{2}(1, 1, -1),$$

and for a bct one as

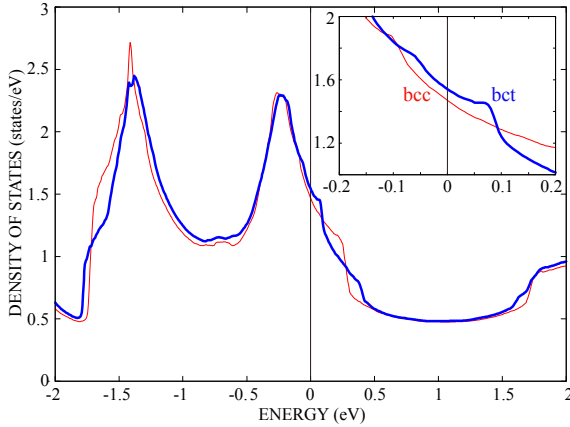$$\mathbf{a}_1 = \frac{a}{2}[-(1 + \delta), 1 + \delta, 1 - \delta],$$

Fig. 18 Calculated electronic density of states of the bcc lattice (thin red curves) and the bct ones (thick blue curves).[33] The inset depicts the magnified portion around the Fermi level.

$$\mathbf{a}_2 = \frac{a}{2}[1 + \delta, -(1 + \delta), 1 - \delta],$$

$$\mathbf{a}_3 = \frac{a}{2}[1 + \delta, 1 + \delta, -(1 - \delta)].$$

Figure 18 depicts the calculated electronic DOS, with the inset depicting the magnification of the low-energy regime. We observe an increase in the DOS at the Fermi level $N(0)$ from the bcc to the bct structures. Here, the value of $N(0)$ is 1.466 (states/eV/atom) for bcc and 1.540 (states/eV/atom) for bct. The order of the present bcc value is reasonably consistent with the past theoretical result.[63]

By the McMillan-Allen-Dynes formula, T_c can be expressed on a quantitative basis as

$$T_c = \frac{\omega_{\ln}}{1.2} \exp\left\{-\frac{1.04(1 + \lambda)}{\lambda - \mu^*(1 + 0.62\lambda)}\right\}, \quad (1)$$

where $\omega_{\ln}$ is the phonon frequency, λ is the electron lattice coupling, and μ^* is the effective Coulomb potential.[64,65] In the case of Nb, λ is of the order of 1, while μ^* is of the order of 0.1.[66] We can pay much attention to λ rather than μ^*.

According to McMillan's theoretical work for strong-coupled superconductors, the electron-phonon coupling of the bcc 4d transition-metal superconductors is strengthened with the increase in $N(0)$.[64] An increase in the electron-phonon coupling constant as well as that in $N(0)$ contribute to the increase in T_c. Consequently, we speculate that the observed $N(0)$ increase due to deformation contributes to the experimental trend of T_c increase.

4.3 Compression effects on V

There is no prominent difference in the change in T_c under HP experiments using Ap-J between HPT-V ($N = 0$) and HPT-V ($N = 10$), and they are consistent with the previous data without using PTM by Ishizuka *et al.*[27] The XRD studies by Jenei *et al.* reported the existence of structural phase transition from bcc to rhombohedral structure around 62 GPa under quasihydrostatic compression in the Ne pressure medium.[67] Under the nonhydrostatic condition, the phase transition occurs at 30 GPa at ambient temperature. Thus, we can assume that the lattice constant monotonically decreases with applying the pressure without the phase transition in the pressure region up to 30 GPa. This trend

basically leads to the decrease in $N(0)$ and T_c. In fact, the experiment exhibits that T_c monotonously increases with an increase in pressure (Fig. 6). Then, the observed increasing trend of T_c in V is not simply described as the effect of $N(0)$. According to superconducting density functional theory, the superconductivity of V seems to be beyond the conventional phonon superconductivity; the theoretical T_c based on the phonon mechanism is much overestimated as 16.3 K compared with the experimental value of 5.4 K.[68] As the possible cause of disagreement, instability of the Cooper pair based on spin fluctuation has been suggested. In general, applying pressure to the system to increase the metallicity would result in suppression of spin fluctuations. Thus, observed positive correlation between the pressure increase and the T_c increase in V might be explained as suppression of the spin fluctuation with pressure increase. Furthermore, the change in spin fluctuation under pressure may mask the effects of strengthening intergrain-contact and slight structural deformation in the unit-cell level. They are important future problems to be investigated.

5. Conclusion

In fifth-group element superconductors V, Nb, and Ta, artificial material manipulation using the severe plastic deformation and additional hydrostatic compression was attempted to increase the superconducting transition temperature T_c. In HPT-Nb with the small N and HPT-Ta for $N = 0$, 2, and 10, the increase in T_c due to strengthening the intergrain contacts was observed. Further, the prominent increase in T_c for HPT-Nb for $N = 10$ originates in the anisotropic deformation of the unit cell. When the quasi-hydrostatic compression is yielded to the material with heavy residual strain in the unit cell, severe strain accumulated in the bcc unit cell with high symmetry is released at a small amount of additional pressure. In the case of Nb, this manner of lattice deformation is favorable for increasing T_c. The knowledge obtained there yields a new strategy to increase T_c from the viewpoints of material science. There would be further potentiality for increasing T_c in the border region between material science using severe plastic deformation and extreme condensed-matter physics using hydrostatic compression.

REFERENCES

1) J.K. Hulm and B.B. Goodman: Phys. Rev. **106** (1957) 659.
2) L.D. Jennings and C.A. Swenson: Phys. Rev. **112** (1958) 31.
3) T.F. Smith: J. Phys. F **2** (1972) 946.
4) M. Strongin: Physica **55** (1971) 155.
5) H. Deguchi, K. Koyama, M. Yasunaka, S. Takagi, N. Nagano and K.

Mizuno: J. Phys. Chem. Solids **63** (2002) 1081.

6) K. Koyama, H. Deguchi, S. Takagi and K. Mizuno: J. Low Temp. Phys. **131** (2003) 595.

7) J. Mayoh and A.M. García-García: Phys. Rev. B **90** (2014) 134513.

8) R. Valiev, Y. Estrin, Z. Horita, T. Langdon, M. Zehetbauer and Y. Zhu: JOM **58**(4) (2006) 33.

9) R. Valiev, R. Islamgaliev and I. Alexandrov: Prog. Mater. Sci. **45** (2000) 103.

10) T. Nishizaki, S. Lee, Z. Horita, T. Sasaki and N. Kobayashi: Physica C **493** (2013) 132.

11) K. Edalati, T. Daio, S. Lee, Z. Horita, T. Nishizaki, T. Akune, T. Nojima and T. Sasaki: Acta Mater. **80** (2014) 149.

12) M. Mito, H. Matsui, K. Tsuruta, T. Yamaguchi, K. Nakamura, H. Deguchi, N. Shirakawa, H. Adachi, T. Yamasaki, H. Iwaoka, Y. Ikoma and Z. Horita: Sci. Rep. **6** (2016) 36337.

13) P.W. Bridgman: Phys. Rev. **48** (1935) 825.

14) N.A. Smirnova, V.I. Levit, V.I. Pilyugin, R.I. Kuznetsov, L.S. Davydova and V.A. Sazonova: Fiz. Met. Metalloved. **61** (1986) 1170.

15) Y. Harai, Y. Ito and Z. Horita: Scr. Mater. **58** (2008) 469.

16) K. Edalati and Z. Horita: Mater. Sci. Eng. A **652** (2016) 325.

17) A. Zhilyaev and T. Langdon: Prog. Mater. Sci. **53** (2008) 893.

18) V.M. Segal, V.I. Reznikov, A.E. Drobyshevskiy and V.I. Kopylov: Russian Metall. **1** (1981) 99.

19) A. Azushima, R. Kopp, A. Korhonen, D.Y. Yang, F. Micari, G.D. Lahoti, P. Groche, J. Yanagimoto, N. Tsuji, A. Rosochowski and A. Yanagida: CIRP Ann. Manuf. Tech. **57** (2008) 716.

20) Y. Saito, H. Utsunomiya, N. Tsuji and T. Sakai: Acta Mater. **47** (1999) 579.

21) J.S. Schilling: *Handbook of High-Temperature Superconductivity*, ed. by J.R. Schrieffer, (Springer, New York, 2007) pp. 427–462.

22) M. Debessai, J.J. Hamlin and J.S. Schilling: Phys. Rev. B **78** (2008) 064519.

23) W.E. Gardner and T.F. Smith: Phys. Rev. **144** (1966) 233.

24) D. Köhnlein: Z. Phys. **208** (1968) 142.

25) N.B. Brabdt and O.A. Zarubia: Sov. Phys. Solid State **15** (1973) 2281.

26) Y. Akahama, M. Kobayashi and H. Kawamura: J. Phys. Soc. Jpn. **64** (1995) 4049.

27) M. Ishizuka, M. Iketani and S. Endo: Phys. Rev. B **61** (2000) R3823.

28) V.V. Struzhkin, Y.A. Timofeev, R.J. Hemley and H.K. Mao: Phys. Rev. Lett. **79** (1997) 4262.

29) W. Gey and G. van Heyden: Z. Phys. **193** (1966) 65.

30) W. Gey: Z. Phys. **229** (1969) 85.

31) N.B. Brandt and E. Papp: Sov. Phys. JETP **30** (1970) 595.

32) T.F. Smith: Phys. Lett. **33** (1970) 465.

33) M. Mito, Y. Kitamura, T. Tajiri, K. Nakamura, R. Shiraishi, K. Ogata, H. Deguchi, T. Yamaguchi, N. Takeshita, T. Nishizaki, K. Edalati and Z. Horita: J. Appl. Phys. **125** (2019) 125901.

34) J. Hatton: Phys. Rev. **103** (1956) 1167.

35) M.D. Fiske: J. Phys. Chem. Solids **2** (1957) 191.

36) S. Lee and Z. Horita: Mater. Trans. **53** (2012) 38.

37) K. Edalati and Z. Horita: Acta Mater. **59** (2011) 6831.

38) K. Edalati, J.M. Cubero-Sesin, A. Alhamidi, I. Mohamed and Z. Horita: Mater. Sci. Eng. A **613** (2014) 103.

39) P. Das, C.V. Tomy, S.S. Banerjee, H. Takeya, S. Ramakrishnan and A.K. Grover: Phys. Rev. B **78** (2008) 214504.

40) T. Nishizaki: private communication (2019).

41) M. Mito, Y. Komorida, H. Tsuruda, J. Tse, S. Desgreniers, Y. Ohishi, A. Leitch, K. Cvrkalj, C. Robertson and R. Oakley: J. Am. Chem. Soc. **131** (2009) 16012.

42) A.A. Leitch, K. Lekin, S.M. Winter, L.E. Downie, H. Tsuruda, J.S. Tse, M. Mito, S. Desgreniers, P.A. Dube, S. Zhang, Q. Liu, C. Jin, Y. Ohishi and R.T. Oakley: J. Am. Chem. Soc. **133** (2011) 6051.

43) H. Tsuruda, M. Mito, H. Deguchi, S. Takagi, A. Leitch, K. Lekin, S. Winter and R. Oakley: Polyhedron **30** (2011) 2997.

44) S. Yamaguchi, N. Yamaguchi, M. Mito, H. Deguchi, P.J. Baker, S.J. Blundell, M.J. Pitcher, D.R. Parker and S.J. Clarke: J. Korean Phys. Soc. **63** (2013) 445.

45) M. Mito, T. Imakyurei, H. Deguchi, K. Matsumoto, H. Hara, T. Ozaki, H. Takeya and Y. Takano: J. Phys. Soc. Jpn. **83** (2014) 023705.

46) M. Mito, H. Matsui, H. Goto, H. Deguchi, K. Matsumoto, H. Hara, T. Ozaki, H. Takeya and Y. Takano: J. Phys. Soc. Jpn. **85** (2016) 024711.

47) M. Mito, K. Ogata, H. Goto, K. Tsuruta, K. Nakamura, H. Deguchi, T. Horide, K. Matsumoto, T. Tajiri, H. Hara, T. Ozaki, H. Takeya and Y. Takano: Phys. Rev. B **95** (2017) 064503.

48) T. Tomita, J.S. Schilling, L. Chen, B.W. Veal and H. Claus: Phys. Rev. B **74** (2006) 064517.

49) M. Mito, M. Hitaka, T. Kawae, K. Takeda, T. Kitai and N. Toyoshima: Jpn. J. Appl. Phys. **40** (2001) 6641.

50) M. Mito: J. Phys. Soc. Jpn. Suppl. A **76** (2007) 182.

51) G.J. Piermarini, S. Block, J.D. Barnett and R.A. Forman: J. Appl. Phys. **46** (1975) 2774.

52) M. Ishizuka: Rev. Sci. Instrum. **76** (2005) 123902.

53) M. Ishizuka, K. Amaya and S. Endo: Rev. Sci. Instrum. **66** (1995) 3307.

54) K. Irie, K. Shibayama, M. Mito, S. Takagi, M. Ishizuka, K. Lekin and R.T. Oakley: Phys. Rev. B **99** (2019) 014417.

55) A. Fujiwara, K. Ishii, T. Watanuki, H. Suematsu, H. Nakao, K. Ohwada, Y. Fujii, Y. Murakami, T. Mori, H. Kawada *et al.*: J. Appl. Cryst. **33** (2000) 1241.

56) T. Varga, A.P. Wilkinson and R.J. Angel: Rev. Sci. Instrum. **74** (2003) 4564.

57) J. Yamauchi, M. Tsukada, S. Watanabe and O. Sugino: Phys. Rev. B **54** (1996) 5586.

58) N. Troullier and J.L. Martins: Phys. Rev. B **43** (1991) 1993.

59) L. Kleinman and D.M. Bylander: Phys. Rev. Lett. **48** (1982) 1425.

60) J.P. Perdew, K. Burke and M. Ernzerhof: Phys. Rev. Lett. **77** (1996) 3865.

61) T. Fujiwara, S. Yamamoto and Y. Ishii: J. Phys. Soc. Jpn. **72** (2003) 777.

62) Y. Nohara, S. Yamamoto and T. Fujiwara: Phys. Rev. B **79** (2009) 195110.

63) K.H. Lee and K.J. Chang: Phys. Rev. B **54** (1996) 1419.

64) W.L. McMillan: Phys. Rev. **167** (1968) 331.

65) P.B. Allen and R.C. Dynes: Phys. Rev. B **12** (1975) 905.

66) R. Akashi, K. Nakamura, R. Arita and M. Imada: Phys. Rev. B **86** (2012) 054513.

67) Z. Jenei, H.P. Liermann, H. Cynn, J.-H.P. Klepeis, B.J. Baer and W.J. Evans: Phys. Rev. B **83** (2011) 054101.

68) N.N. Lathiotakis, M.A.L. Marques, M. Lüders, L. Fast and E.K.U. Gross: Int. J. Quantum Chem. **99** (2004) 790.